LETTER

doi:10.1038/nature11505

Stabilizing Rabi oscillations in a superconducting qubit using quantum feedback

R. Vijay[1], C. Macklin[1], D. H. Slichter[1]†, S. J. Weber[1], K. W. Murch[1], R. Naik[1], A. N. Korotkov[2] & I. Siddiqi[1]

The act of measurement bridges the quantum and classical worlds by projecting a superposition of possible states into a single (probabilistic) outcome. The timescale of this 'instantaneous' process can be stretched using weak measurements[1,2], such that it takes the form of a gradual random walk towards a final state. Remarkably, the interim measurement record is sufficient to continuously track and steer the quantum state using feedback[3–8]. Here we implement quantum feedback control in a solid-state system, namely a superconducting quantum bit (qubit) coupled to a microwave cavity[9]. A weak measurement of the qubit is implemented by probing the cavity with microwave photons, maintaining its average occupation at less than one photon. These photons are then directed to a high-bandwidth, quantum-noise-limited amplifier[10,11], which allows real-time monitoring of the state of the cavity (and, hence, that of the qubit) with high fidelity. We demonstrate quantum feedback control by inhibiting the decay of Rabi oscillations, allowing them to persist indefinitely[12]. Such an ability permits the active suppression of decoherence and enables a method of quantum error correction based on weak continuous measurements[13,14]. Other applications include quantum state stabilization[4,7,15], entanglement generation using measurement[16], state purification[17] and adaptive measurements[18,19].

Feedback protocols in classical systems, from antilock brakes to pacemakers, use the outcome of a measurement to stabilize the system about a desired state. The operation of such feedback protocols is predicated on the idea that measurement does not alter the state of the system. This is no longer true in quantum mechanics, where measurement is necessarily invasive[1]. In the Copenhagen interpretation, a quantum object can exist simultaneously in more than one eigenstate of the measurement operator until observed—Schrödinger's celebrated 'dead-and-alive' cat being the quintessential hypothetical example[20]. The reality of the situation is established by the act of measurement, which forces the system 'instantaneously' into one of these eigenstates in a probabilistic fashion (the 'measurement back-action'). Therefore, this back-action must be accounted for when developing a feedback protocol to stabilize a quantum system, such as a qubit.

One solution is to use weak measurements[1,2], where the rate ($\Gamma_{\rm meas}$) at which information is extracted is deliberately limited, thereby slowing down the qubit's random walk towards an eigenstate. Integral to this scheme is a detector with efficiency $\eta_{\rm det} = \Gamma_{\rm meas}/\Gamma_\varphi \approx 1$, where Γ_φ is the ensemble-averaged dephasing rate due to measurement back-action[21]. The high detector efficiency allows us to track the qubit continuously, and steer it to a desired state using real-time feedback.

The experimental set-up is shown in Fig. 1. Our quantum system (Fig. 1b) is an anharmonic oscillator realized by a capacitively shunted Josephson junction, dispersively coupled to a three-dimensional microwave cavity[22]. We use its two lowest energy levels to form a qubit (transmon[23]) with a transition frequency of $\omega_{01}/2\pi = 5.4853$ GHz. The cavity resonant frequency with the qubit in the ground state is $\omega_c/2\pi = 7.2756$ GHz. The strongly coupled output port sets the cavity linewidth $\kappa/2\pi = 13.4$ MHz, and control and measurement signals are injected via the weakly coupled input port (Fig. 1a, b). The qubit–cavity coupling results in a state-dependent phase shift ($\Delta\phi = 2\tan^{-1}(2\chi/\kappa) = 12^\circ$, $\chi/2\pi = 0.687$ MHz) of the cavity output field[9,24], with the state information contained in one quadrature of the signal. The cavity output is sent to a near-noiseless ($\eta_{\rm det} \approx 1$) phase-sensitive parametric

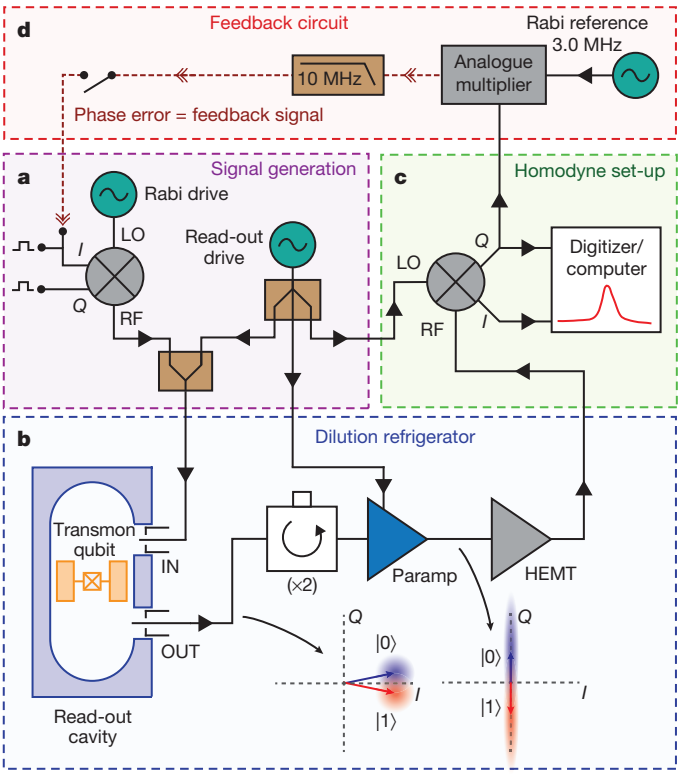

Figure 1 | Experimental set-up. **a**, Signal generation set-up. One generator provides the Rabi drive at the a.c. Stark-shifted qubit frequency ($\omega_{01} - 2\chi\bar{n}$), and the output of another generator at 7.2749 GHz is split to create the measurement signal, paramp drive and local oscillator. The relative amplitudes and phases of these three signals are controlled by variable attenuators and phase shifters (not shown). *I*, in-phase component; *Q*, quadrature component; LO, local oscillator; RF, radio frequency. **b**, Simplified version of the cryogenic part of the experiment; all components are at 30 mK (except for the high-electron-mobility transistor (HEMT) amplifier, which is at 4 K). The combined qubit and measurement signals enter the weakly coupled cavity port, interact with the qubit and leave from the strongly coupled port. The output passes through two isolators (which protect the qubit from the strong paramp drive), is amplified and then continues to the demodulation set-up. The coherent state at the output of the cavity for the ground and excited states is shown schematically before and after parametric amplification. **c**, **d**, The amplified signal is homodyne-detected and the two quadratures are digitized (**c**). The amplified quadrature (*Q*) is split off and sent to the feedback circuit (**d**), where it is multiplied with the Rabi reference signal. The product is low-pass-filtered and fed back to the *IQ* mixer in **a** to modulate the Rabi drive amplitude.

[1]Quantum Nanoelectronics Laboratory, Department of Physics, University of California, Berkeley, California 94720, USA. [2]Department of Electrical Engineering, University of California, Riverside, California 92521, USA. †Present address: Time and Frequency Division, National Institute of Standards and Technology, Boulder, Colorado 80305, USA.

amplifier[10,11] (paramp), which boosts the relevant quadrature to a level compatible with classical circuitry. The paramp output is further amplified and homodyne-detected (Fig. 1c) such that the amplified quadrature (Q) contains the final measurement signal.

We obtain Rabi oscillations with the cavity continuously excited at $\omega_r/2\pi = 7.2749$ GHz ($\omega_r \approx \omega_c - \chi$) with a mean cavity photon occupation ($\bar{n}$) that controls the measurement strength (see Supplementary Information, section II, for calibration of $\bar{n}$). The Rabi drive at the a.c. Stark-shifted[25] qubit frequency ($\omega_{01} - 2\chi\bar{n}$) is turned on for a fixed duration, τ_m. The amplitude is adjusted to yield a Rabi frequency of $\Omega_R/2\pi = 3$ MHz. First we average 10^4 measurement traces to obtain a conventional ensemble-averaged Rabi oscillation trace (Fig. 2a). Even though the qubit is continuously oscillating between its ground and excited states, the oscillation phase diffuses, primarily owing to measurement back-action. As a result, the averaged oscillation amplitude decays over time, but the frequency domain response retains a signature of these oscillations[26]. We Fourier-transform the individual measurement traces and plot the averaged spectrum (Fig. 2b, blue trace). A peak, centred at 3 MHz and with a full-width at half-maximum of $\Gamma/2\pi$, is observed and remains unchanged even when τ_m is much longer than the decay time of the ensemble-averaged oscillations. A plot of $\Gamma/2\pi$ for different measurement strengths (in units of $\bar{n}$) is shown in Fig. 2c. As expected in the dispersive regime, Γ and $\bar{n}$ are linearly related[25]. The vertical offset is dominated by pure environmental dephasing, $\Gamma_{env}/2\pi$, but has contributions from qubit relaxation (T_1) and thermal excitation into higher qubit levels; more details can be found in Supplementary Information, sections II and IV(C).

The ratio of the height of the Rabi spectral peak to the height of the noise floor has a theoretical maximum value of four[27], corresponding to an ideal measurement with overall efficiency $\eta = 1$. For our set-up, this efficiency can be separated into two contributions as $\eta = \eta_{det}\eta_{env}$. The detector efficiency is given by $\eta_{det} = (1+2n_{add})^{-1}$, with n_{add} being the number of noise photons added by the amplification chain. The added noise is referenced to the output of the cavity and includes the effect of signal attenuation between the cavity and the paramp. The effect of environmental dephasing, Γ_{env}, is modelled using $\eta_{env} = (1+\Gamma_{env}/\Gamma_\varphi)^{-1}$. The best measurement efficiency we obtain experimentally is $\eta = 0.40$, with $\eta_{det} = 0.46$ and $\eta_{env} = 0.87$; more details can be found in Supplementary Information, section III.

We now discuss the quantum feedback protocol, which is motivated by the classical phase-locked loop used for stabilizing an oscillator. The amplified quadrature is multiplied by a Rabi reference signal with frequency $\Omega_0/2\pi = 3$ MHz using an analogue multiplier (Fig. 1d). The output of this multiplier is low-pass-filtered and yields a signal proportional to the sine of the phase difference, θ_{err}, between the 3-MHz reference and the 3-MHz component of the amplified quadrature. This 'phase error' signal is fed back to control the Rabi frequency Ω_R by modulating the Rabi drive strength with an upconverting IQ mixer (Fig. 1a). The amplitude of the reference signal controls the dimensionless feedback gain, F, through the expression $\Omega_{fb}/\Omega_R = -F\sin(\theta_{err})$, where Ω_{fb} is the change in Rabi frequency due to feedback. Figure 2d shows the ensemble-averaged, feedback-stabilized oscillation, which persists for much longer than the original oscillation in Fig. 2a. In fact, within the limits imposed by our maximum data acquisition time of 20 ms, these oscillations persist indefinitely. The red trace in Fig. 2b shows the corresponding averaged spectra. The needle-like peak at 3 MHz is the signature of the stabilized Rabi oscillations.

To confirm the quantum nature of the feedback-stabilized oscillations, we perform state tomography on the qubit[28]. We stabilize the dynamical qubit state, stop the feedback and Rabi driving after a fixed time (80 μs + τ_{tomo} after starting the Rabi drive), and then measure the projection of the quantum state along one of three orthogonal axes. This is done using strong measurements (by increasing $\bar{n}$) with high single-shot fidelity[11]. This allows us to remove any data points where the qubit was found in the second excited state (Supplementary Information, section IV(C)). By repeating this many times, we can determine $\langle\sigma_X\rangle$, $\langle\sigma_Y\rangle$ and $\langle\sigma_Z\rangle$,

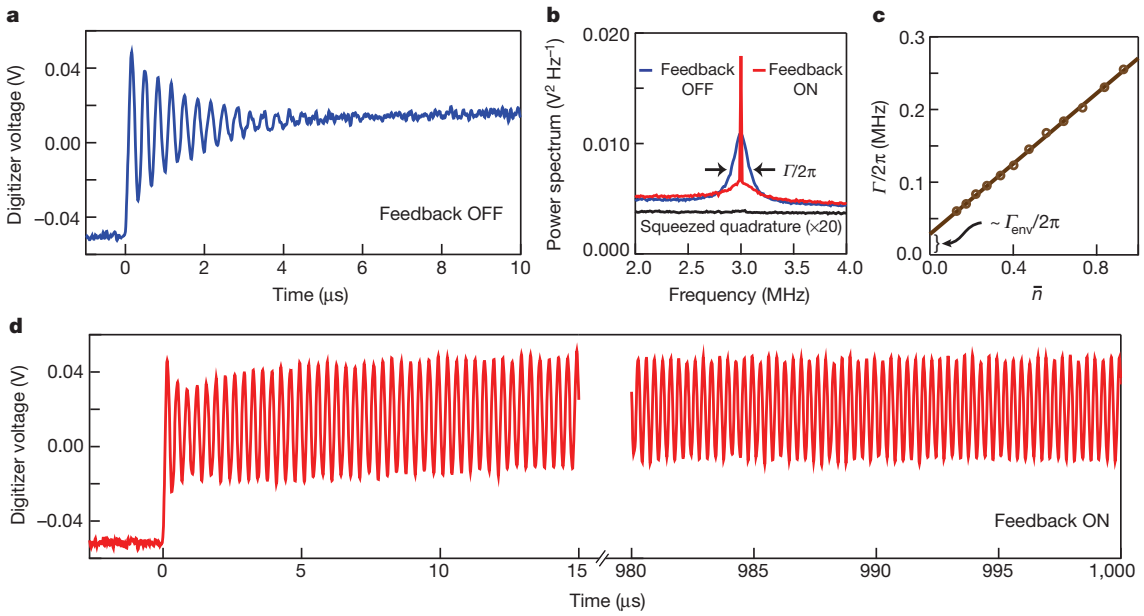

Figure 2 | Rabi oscillations and feedback. **a**, We average 10^4 measurement traces using weak continuous measurement and simultaneous Rabi driving to obtain ensemble-averaged Rabi oscillations that decay in time as a result of ensemble dephasing. **b**, Averaged Fourier transforms of the individual measurement traces from **a**. The spectrum shows a peak at the Rabi frequency (blue trace) with a full-width at half-maximum of $\Gamma/2\pi$. The grey trace shows an identically prepared spectrum for the squeezed quadrature (multiplied by 20 for clarity), which contains no qubit state information. **c**, $\Gamma/2\pi$ plotted as a function of cavity photon occupation, $\bar{n}$ (measurement strength), showing the expected linear dependence. The vertical offset is dominated by pure environmental dephasing, $\Gamma_{env}/2\pi$, but has contributions from qubit relaxation (T_1) and thermal excitation into higher qubit levels. **d**, Feedback-stabilized, ensemble-averaged Rabi oscillations, which persist for much longer times than those without feedback (**a**). The corresponding spectrum, shown in **b**, has a needle-like peak at the Rabi reference frequency (red trace). The slowly changing mean level in the Rabi oscillation traces in **a** and **d** is due to the thermal transfer of population into the second excited state of the qubit. See Supplementary Information, section IV(C), for more details.

the three components of the Bloch vector for the ensemble qubit state. Figure 3a shows a plot of the Bloch vector components for different time points (τ_{tomo}) over one oscillation period ($2\pi\Omega_0$). The Y and Z components are well fitted by a sinusoidal function, whereas the X component is nearly zero as expected for a coherent Rabi oscillation about the X axis. The imperfect efficiency of the feedback process is reflected in the non-unit amplitude of these oscillations. This feedback efficiency, D, is given by the time-averaged scalar product of the desired and actual state vectors on the Bloch sphere (Supplementary Information, section IV(A)). In our experiment, the measurement is weak enough that the stabilized oscillations are sinusoidal and D is approximately equal to the amplitude of these oscillations.

In Fig. 3b, we plot D (red squares) versus the dimensionless feedback gain, F. We find a maximum value of $D = 0.45$ for the optimal choice of F. Ideally, feedback efficiency improves with measurement strength ($\eta_{env} \rightarrow 1$) but requires correspondingly larger feedback loop bandwidth. Thus, in the presence of finite feedback bandwidth and loop delay, there exists an optimal measurement strength, which for our experiment was $\Gamma_\varphi/2\pi = 0.134$ MHz. The dashed black line in Fig. 3b is a plot of the theoretical expression for D, given by

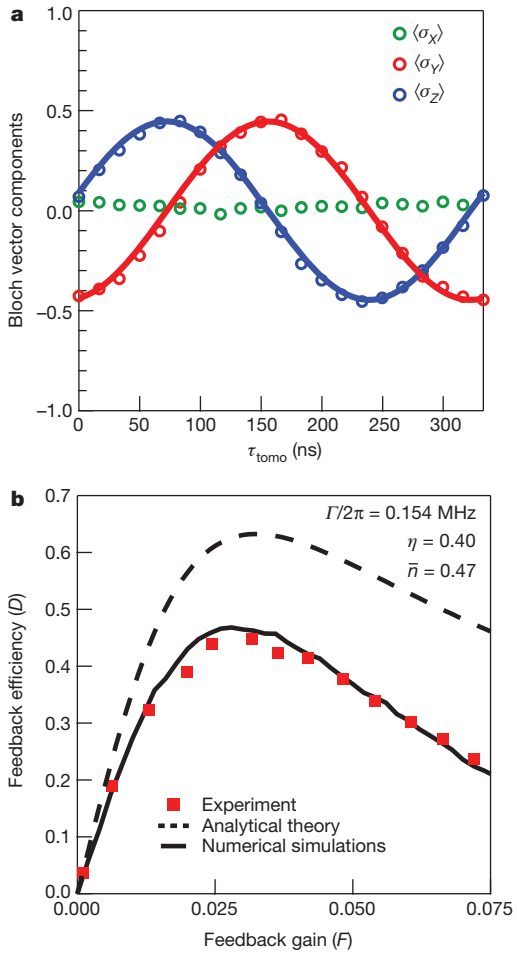

Figure 3 | Tomography and feedback efficiency. **a**, Quantum state tomography of the feedback-stabilized state. We plot $\langle\sigma_X\rangle$, $\langle\sigma_Y\rangle$ and $\langle\sigma_Z\rangle$ for different time points τ_{tomo} in one full Rabi oscillation of the qubit. The solid lines are sinusoidal fits. The magnitude of these sinusoidal oscillations is approximately equal to the feedback efficiency, $D = 0.45$. **b**, D plotted as a function of the dimensionless feedback gain, F. Solid red squares show experimental data with a maximum value of $D = 0.45$. The dashed black line is a plot of equation (1) with $\eta = 0.40$ and $\Gamma/2\pi = 0.154$ MHz ($\bar{n} = 0.47$, $\Gamma_{env}/2\pi = 0.020$ MHz), whereas the solid black line is obtained from full numerical simulations of the Bayesian equations including finite loop delay (250 ns) and feedback bandwidth (10 MHz).

$$D = 2\left(\frac{1}{\eta}\frac{F}{\Gamma/\Omega_0} + \frac{\Gamma/\Omega_0}{F}\right)^{-1} \quad (1)$$

and is derived using a simple analytical theory based on the Bayesian formalism for the qubit state trajectory (Supplementary Information, section IV(A)). This expression does not account for finite feedback bandwidth, loop delays in the circuit or qubit relaxation. The maximum value, $D_{max} = \sqrt{\eta}$, is obtained for an optimal feedback gain of $F_{opt} = \sqrt{\eta}\Gamma/\Omega_0$. A value of $D_{max} < 1$ implies that the stabilized state is a mixed state; this occurs for $\eta < 1$, implying that we have incomplete information about the qubit state. To account for the finite loop delay (250 ns), feedback bandwidth (10 MHz) and qubit relaxation ($T_1 = 20$ μs), we performed full numerical simulations of the Bayesian equations for qubit evolution (Supplementary Information, section IV(B)). The results are shown as a black solid line in Fig. 3b and agree well with our experimental data.

In our experiment, even though the system being controlled is quantum and subject to measurement back-action, we essentially treat it as a classical oscillator and successfully apply a feedback protocol based completely on classical intuition. This can be done because the feedback signal achieves near-perfect cancellation of the random measurement back-action for optimal F. Although it is not true in general, in this particular scheme improvements in the feedback efficiency from full reconstruction of the quantum state[8] are small. Furthermore, it is possible to approach a pure state with $D = 1$ by ensuring that $\eta = 1$ and eliminating feedback loop delay.

We have demonstrated a continuous analogue feedback scheme to stabilize Rabi oscillations in a superconducting qubit, allowing them to persist indefinitely. The efficiency of the feedback is limited primarily by signal attenuation and loop delay, and could be improved in the near future with the development of on-chip paramps and cryogenic electronics to lessen the effects of attenuation and delay, respectively. We anticipate that our present technology can be extended to entangled qubits to provide another route to quantum error correction based on weak continuous measurements[13,14]. Such methods might be advantageous in architectures where strong measurements can cause qubit state mixing[29]. This development may be the start of a new era of measurement-based quantum control for solid-state quantum information processing[4,7,15–19].

METHODS SUMMARY

The transmon qubit was fabricated on a bare, high-resistivity Si wafer using electron-beam lithography and double-angle aluminium evaporation with an intervening oxidation step. The qubit is a single Josephson junction connecting two rectangular paddles (420 μm × 600 μm) that provide the shunting capacitance and coupling to the cavity. The cavity was machined out of 6061 aluminium alloy. The quality factor of the cavity was adjusted by controlling the length of the centre conductor of the SMA coaxial connector protruding into the cavity volume. These lengths were chosen to give strong coupling at the output port and weak coupling at the input port, resulting in a net power transmission on resonance of −20 to −30 dB. Qubit rotations around the X and Y axes of the Bloch sphere for state tomography were performed using resonant microwave pulses. The strong measurement used in state tomography was implemented with a 800-ns read-out pulse with an amplitude corresponding to a mean cavity occupation of $\bar{n} \approx 11$.

Received 18 May; accepted 17 August 2012.

1. Wiseman, H. M. & Milburn, G. J. *Quantum Measurement and Control* (Cambridge Univ. Press, 2009).
2. Gardiner, C. W. & Zoller, P. *Quantum Noise* (Springer, 2004).
3. Wiseman, H. M. & Milburn, G. J. Quantum theory of optical feedback via homodyne detection. *Phys. Rev. Lett.* **70,** 548–551 (1993).
4. Hofmann, H. F., Mahler, G. & Hess, O. Quantum control of atomic systems by homodyne detection and feedback. *Phys. Rev. A* **57,** 4877–4888 (1998).
5. Korotkov, A. N. Selective quantum evolution of a qubit state due to continuous measurement. *Phys. Rev. B* **63,** 115403 (2001).
6. Smith, W. P., Reiner, J. E., Orozco, L. A., Kuhr, S. & Wiseman, H. M. Capture and release of a conditional state of a cavity QED system by quantum feedback. *Phys. Rev. Lett.* **89,** 133601 (2002).
7. Gillett, G. G. *et al.* Experimental feedback control of quantum systems using weak measurements. *Phys. Rev. Lett.* **104,** 080503 (2010).

8. Sayrin, C. *et al.* Real-time quantum feedback prepares and stabilizes photon number states. *Nature* **477,** 73–77 (2011).
9. Blais, A., Huang, R.-S., Wallraff, A., Girvin, S. M. & Schoelkopf, R. J. Cavity quantum electrodynamics for superconducting electrical circuits: an architecture for quantum computation. *Phys. Rev. A* **69,** 062320 (2004).
10. Hatridge, M., Vijay, R., Slichter, D. H., Clarke, J. & Siddiqi, I. Dispersive magnetometry with a quantum limited SQUID parametric amplifier. *Phys. Rev. B* **83,** 134501 (2011).
11. Vijay, R., Slichter, D. H. & Siddiqi, I. Observation of quantum jumps in a superconducting artificial atom. *Phys. Rev. Lett.* **106,** 110502 (2011).
12. Ruskov, R. & Korotkov, A. N. Quantum feedback control of a solid-state qubit. *Phys. Rev. B* **66,** 041401 (2002).
13. Ahn, C., Doherty, A. C. & Landahl, A. J. Continuous quantum error correction via quantum feedback control. *Phys. Rev. A* **65,** 042301, 2002..
14. Tornberg, L. & Johansson, G. High-fidelity feedback-assisted parity measurement in circuit QED. *Phys. Rev. A* **82,** 012329 (2010).
15. Wang, J. & Wiseman, H. M. Feedback-stabilization of an arbitrary pure state of a two-level atom. *Phys. Rev. A* **64,** 063810 (2001).
16. Ruskov, R. & Korotkov, A. N. Entanglement of solid-state qubits by measurement. *Phys. Rev. B* **67,** 241305 (2003).
17. Combes, J. & Jacobs, K. Rapid state reduction of quantum systems using feedback control. *Phys. Rev. Lett.* **96,** 010504 (2006).
18. Jacobs, K. Feedback control for communication with non-orthogonal states. *Quantum Inf. Comput.* **7,** 127–138 (2007).
19. Cook, R. L., Martin, P. J. & Geremia, J. M. Optical coherent state discrimination using a closed-loop quantum measurement. *Nature* **446,** 774–777 (2007).
20. Schrödinger, E. The present situation in quantum mechanics. *Proc. Am. Phil. Soc.* **124,** 323–338 (1980).
21. Clerk, A. A., Devoret, M. H., Girvin, S. M., Marquardt, F. & Schoelkopf, R. J. Introduction to quantum noise, measurement, and amplification. *Rev. Mod. Phys.* **82,** 1155–1208 (2010).
22. Paik, H. *et al.* Observation of high coherence in Josephson junction qubits measured in a three-dimensional circuit QED architecture. *Phys. Rev. Lett.* **107,** 240501 (2011).
23. Koch, J. *et al.* Charge-insensitive qubit design derived from the Cooper pair box. *Phys. Rev. A* **76,** 042319 (2007).
24. Wallraff, A. *et al.* Approaching unit visibility for control of a superconducting qubit with dispersive readout. *Phys. Rev. Lett.* **95,** 060501 (2005).
25. Schuster, D. I. *et al.* ac Stark shift and dephasing of a superconducting qubit strongly coupled to a cavity field. *Phys. Rev. Lett.* **94,** 123602 (2005).
26. Palacios-Laloy, A. *et al.* Experimental violation of a Bell's inequality in time with weak measurement. *Nature Phys.* **6,** 442–447 (2010).
27. Korotkov, A. N. & Averin, D. V. Continuous weak measurement of quantum coherent oscillations. *Phys. Rev. B* **64,** 165310 (2001).
28. Steffen, M. *et al.* State tomography of capacitively shunted phase qubits with high fidelity. *Phys. Rev. Lett.* **97,** 050502 (2006).
29. Slichter, D. H. *et al.* Measurement-induced qubit state mixing in circuit QED from upconverted dephasing noise. Preprint at http://arxiv.org/abs/1206.6946 (2012).

Supplementary Information is available in the online version of the paper.

Acknowledgements We thank M. Sarovar for several discussions and Z. Minev for assistance with numerical simulations. This research was supported in part (R.V., C.M. and I.S.) by the US Army Research Office (W911NF-11-1-0029) and the Office of the Director of National Intelligence (ODNI), Intelligence Advanced Research Projects Activity (IARPA), through the Army Research Office (K.W.M., S.J.W. and A.N.K.). All statements of fact, opinion or conclusions contained herein are those of the authors and should not be construed as representing the official views or policies of IARPA, the ODNI or the US government. D.H.S. acknowledges support from a Hertz Foundation Fellowship endowed by Big George Ventures. A.N.K. also acknowledges funding from an ARO MURI.

Author Contributions R.V., C.M. and D.H.S. performed the experiment, which is based on a proposal by A.N.K. R.V. analysed the data, performed numerical simulations and wrote the manuscript. S.J.W. and K.W.M. fabricated the qubit and cavity. R.N. helped with cavity design by performing electromagnetic simulations. A.N.K. provided theoretical support and helped with numerical simulations. All authors helped in editing the manuscript. All work was carried out under the supervision of I.S.

Author Information Reprints and permissions information is available at www.nature.com/reprints. The authors declare no competing financial interests. Readers are welcome to comment on the online version of the paper. Correspondence and requests for materials should be addressed to R.V. (rvijay@berkeley.edu) or I.S. (irfan@berkeley.edu).